Data-Driven LIDAR Feedforward Predictive Wind Turbine Control

Dinkla, Rogier; Oomen, Tom; Wingerden, Jan Willem Van; Mulders, Sebastiaan P.

DOI
10.1109/CCTA54093.2023.10252439

Publication date
2023

Document Version
Final published version

Published in
Proceedings of the 2023 IEEE Conference on Control Technology and Applications, CCTA 2023

2023 IEEE Conference on Control Technology and Applications (CCTA)
August 16-18, 2023. Bridgetown, Barbados

Data-Driven LIDAR Feedforward Predictive Wind Turbine Control

Rogier Dinkla[1], Tom Oomen[1,2], Jan-Willem van Wingerden[1], Sebastiaan P. Mulders[1]

2023 IEEE Conference on Control Technology and Applications (CCTA) | 979-8-3503-3544-6/23/$31.00 ©2023 IEEE | DOI: 10.1109/CCTA54093.2023.10252439

***Abstract*— Light Detection and Ranging (LIDAR)-assisted Model Predictive Control (MPC) for wind turbine control has received much attention for its ability to incorporate future wind speed disturbance information in a receding horizon optimal control problem. However, the growth of wind turbine sizes results in increasing system complexity and system interactions, and complicates the design of model-based controllers like MPC. Together with increasing data availability, this obstacle motivates the use of direct data-driven predictive control approaches like Subspace Predictive Control (SPC). An SPC implementation is developed that both does not suffer from traditional, potentially detrimental closed-loop identification bias and incorporates past and future (not necessarily periodic) disturbance information. Simulations of the presented method for above-rated wind turbine rotor speed regulation using pitch control demonstrate the capabilities of the data-driven SPC algorithm for increasing degrees of wind speed disturbance information in the developed framework.**

I. INTRODUCTION

State-of-the art wind turbine control methods facilitate the design and operation of modern large, flexible wind turbines, the development of which makes wind energy an increasingly economically attractive sustainable alternative to fossil fuels. With this in mind, opportunities to (more) effectively leverage data from, e.g., forecasting methods offer an interesting avenue of further investigation [1].

Such methods can be used to complement essential feedback strategies in classical wind turbine control applications, which suffers from important practical limitations. For instance, a noteworthy feedback limitation for turbine rotational speed regulation stems from the considerable phase delay imposed by the increasingly large inertia of larger wind turbine rotors. Moreover, pitch actuator delays are known to limit the effectiveness of above-rated fatigue load mitigation when relying on feedback [2]. Meanwhile, the development of more cost effective and reliable Light Detection and Ranging (LIDAR) technology (see Fig. 1) has made it reasonable to consider future wind speeds as measurable disturbances [3], prompting the investigation of various wind turbine applications that additionally employ feedforward control. The potential of future wind speed information for control purposes has been demonstrated by means of scaled [4] and full-scale experiments [5], [6].

Future wind speed information from LIDAR is most frequently employed using Model Predictive Control (MPC) [7]. The ability to compute an optimal future input trajectory when provided with a suitable cost function and previewed wind speed trajectory as well as its ability to handle constraints and multiple-input, multiple-output systems makes MPC an appealing wind turbine control method. Whilst extensive literature on LIDAR-assisted MPC for wind turbines exists (an overview can be gleaned from reviews of LIDAR-assisted control found within [7], [8], [9] and the references in [4]), experimental implementations of such schemes (whether scaled or at full-scale) remain rare [4], [10]. As a reason for this, consider that accurate modelling of wind turbines is becoming more difficult due to their higher complexity [7] as a result of, e.g., dynamic coupling arising from increasingly flexible components [11]. In fact, recent experience with MPC implementations for wind turbines in the field indicates that obtaining models that strike a good balance between accuracy, complexity (for real-time feasibility), and robustness makes turbine commissioning a challenging and tedious process [10].

The inherent wind turbine modelling difficulties encoun-

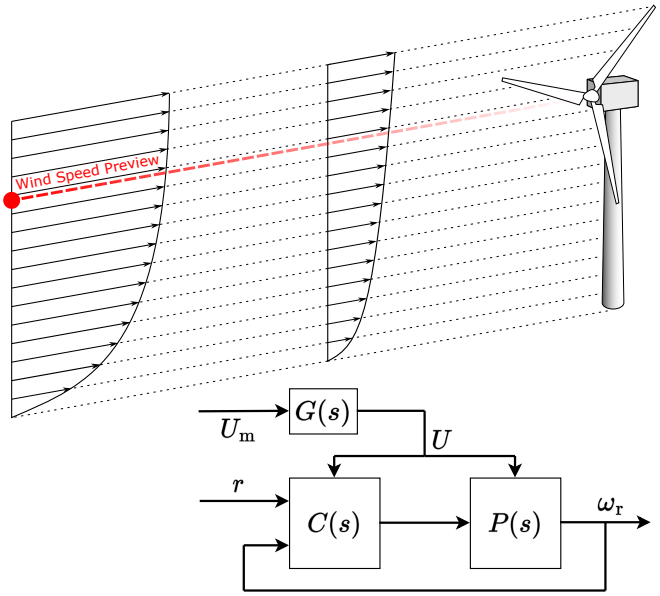

Fig. 1: Light Detection and Ranging (LIDAR) can provide measurements of the wind speed U_m ahead of the turbine (indicated by the red dot). Propagation effects (like delay) of the measured wind speed U_m to the rotor effective wind speed U are captured by the transfer function $G(s)$. The rotor effective wind speed acts on the wind turbine $P(s)$ and is available to the controller $C(s)$ together with future wind speed predictions to, e.g., regulate the rotor speed ω_r to a reference r.

[1]Delft Center for Systems and Control, Faculty of Mechanical Engineering, Delft University of Technology, Mekelweg 2, 2628 CD Delft, The Netherlands {R.T.O.Dinkla, T.A.E.Oomen, J.W.vanWingerden, S.P.Mulders}@tudelft.nl
[2]Control Systems Technology Group, Department of Mechanical Engineering, Eindhoven University of Technology, 5600 MB Eindhoven, The Netherlands

tered with LIDAR-assisted MPC applications, together with the increasing availability of data, motivate the use of direct data-driven predictive control techniques. Direct data-driven methods synthesize a controller from data without obtaining a specific system model realization in the process. Such approaches can thereby outperform their model-based counterparts, particularly when the true system dynamics are only captured by higher order models (implying that under-modelling is unavoidable) [12], as is increasingly true for wind turbines.

An example of a direct data-driven predictive control method that has raised considerable attention is Data-enabled Predictive Control (DeePC), which was originally developed in [13] and takes a behavioural systems theoretical approach that is based on Willems' fundamental Lemma [14]. In the presence of noise, this method has been shown to be equivalent (using regularizations [15] and instrumental variables [16]) to another data-driven control method called Subspace Predictive Control (SPC) as developed in [17]. Unfortunately, the traditional algorithms suffer from closed-loop identification bias in the presence of noise [18], which can be detrimental to their performance [19]. A specific closed-loop SPC method was developed in [20] to address this problem.

Literature of direct data-driven predictive wind turbine control that considers future disturbances focuses on Subspace Predictive Repetitive Control (SPRC) (see [21]). It extends closed-loop SPC from [20] by considering disturbances to be periodic. Given the periodic nature of many wind-induced turbine loads it has mainly seen applications related to periodic load mitigation.

For rotational speed regulation, approximating the wind speed as a periodic disturbance is not realistic, and hence the regulation error may be amplified [22]. To the best of the author's knowledge, the only application of closed-loop direct data-driven predictive wind turbine control that leverages future wind speed information for rotational speed regulation is found in [23]. Therein the authors validate closed-loop SPC using upstream wind speed measurements on a scaled turbine that uses torque control at below-rated conditions. The potential of closed-loop SPC for above-rated pitch control using future wind speed information thus remains unexplored. Moreover, the precise mechanism by which feedforward is incorporated in the controller is not explained. In [24] the authors incorporate measurable disturbance information for SPC, but they do not apply a closed-loop approach and do not consider future disturbance information to be available.

Considering the above, this paper's contributions are:

1) The derivation of a *closed-loop* direct data-driven predictive control algorithm (in the form of SPC) that employs feedforward control by incorporating information on future disturbances (that need not be periodic).
2) Demonstration by means of simulation of the developed algorithm on a wind turbine for rotor speed regulation at *above-rated* conditions using pitch control. The performance of three controllers with different degrees of wind speed information is compared to assess the use of future disturbance information within the developed framework.

This paper has the following structure. In Section II a closed-loop SPC framework that can incorporate future (wind speed) disturbance information is presented. Subsequently, Section III demonstrates the performance of three such controllers that exploit differing levels of previewed wind speed information for the purpose of rotor speed regulation. Two wind cases are considered, both for above rated-power operating conditions: one with a Mexican hat wind gust and one with a turbulent wind speed profile. At the end, conclusions and suggestions for future work are discussed in Section IV.

II. Closed-loop SPC with Future Disturbances

This section derives the closed-loop SPC framework that takes into account past and future disturbances. As will be shown later, the incorporation of such information is shown to significantly improve the disturbance rejection of the proposed control method.

A. Model Structure

A linear time-invariant (LTI) discrete state space system with disturbances and both process and measurement noise is considered in innovation form:

$$x_{k+1} = Ax_k + B_{\mathrm{u}}u_k + B_{\mathrm{d}}d_k + Ke_k, \tag{1a}$$

$$y_k = Cx_k + D_{\mathrm{u}}u_k + D_{\mathrm{d}}d_k + e_k, \tag{1b}$$

where $x_k \in \mathbb{R}^n$, $u_k \in \mathbb{R}^r$, $d_k \in \mathbb{R}^q$, and $y_k \in \mathbb{R}^l$ are respectively the state, input, disturbance, and output vectors, and $e_k \in \mathbb{R}^l$ represents ergodic zero-mean, white innovation noise with covariance $\mathbb{E}\{e_i e_j^\top\} = W\delta_{ij}$, with $W > 0$. The disturbance inputs are considered apart from the control inputs as they are not controllable. Moreover, $\{A, B_{\mathrm{u}}, B_{\mathrm{d}}, C, D_{\mathrm{u}}, D_{\mathrm{d}}, K\}$ are matrices of appropriate dimensions, and $k \in \mathbb{Z}$ is a time index. For this form to be admissible it is assumed that the pair (A, C) is observable, that $A-KC$ has all its eigenvalues inside the unit circle, and that the pair $(A, \begin{bmatrix} B_{\mathrm{u}} & B_{\mathrm{d}} & KW^{1/2} \end{bmatrix})$ is controllable. For the purpose of consistent system identification, it is furthermore assumed here that the input and disturbance trajectories are quasi-stationary [25].

By manipulation of (1), the system can alternatively be represented in the predictor form, given by

$$x_{k+1} = \widetilde{A}x_k + \widetilde{B}_{\mathrm{u}}u_k + \widetilde{B}_{\mathrm{d}}d_k + Ky_k, \tag{2a}$$

$$y_k = Cx_k + D_{\mathrm{u}}u_k + D_{\mathrm{d}}d_k + e_k, \tag{2b}$$

in which $\begin{bmatrix} \widetilde{B}_{\mathrm{u}} & \widetilde{B}_{\mathrm{d}} \end{bmatrix} = [B_{\mathrm{u}}\ B_{\mathrm{d}}] - K[D_{\mathrm{u}}\ D_{\mathrm{d}}]$, and $\widetilde{A} = A - KC$.

B. Notation

Before proceeding with the derivation of the data equations for the closed-loop SPC algorithm, several frequently-used

matrices are defined next. First, a recurring block-Toeplitz matrix is defined as:

$$\mathcal{T}_s(\mathcal{A},\mathcal{B},\mathcal{C},\mathcal{D}) = \begin{bmatrix} \mathcal{D} & 0 & 0 & \dots & 0 \\ \mathcal{CB} & \mathcal{D} & 0 & \dots & 0 \\ \mathcal{CAB} & \mathcal{CB} & \mathcal{D} & \dots & 0 \\ \vdots & \vdots & \ddots & \ddots & \vdots \\ \mathcal{CA}^{s-2}\mathcal{B} & \mathcal{CA}^{s-3}\mathcal{B} & \dots & \mathcal{CB} & \mathcal{D} \end{bmatrix},$$

with the matrices $\mathcal{A}$, $\mathcal{B}$, $\mathcal{C}$, and $\mathcal{D}$ all of compatible dimensions, and a number of block-rows that is indicated by the subscript s. Using a strictly-positive integer prediction window length $f \in \mathbb{Z}^+$, the above-given block-Toeplitz matrix definition is used to define

$$\mathcal{T}_f^{\mathrm{u}} = \mathcal{T}_f(A, B_{\mathrm{u}}, C, D_{\mathrm{u}}), \quad \mathcal{T}_f^{\mathrm{d}} = \mathcal{T}_f(A, B_{\mathrm{d}}, C, D_{\mathrm{d}})$$
$$\mathcal{H}_f = \mathcal{T}_f(A, K, C, I), \qquad \widetilde{\mathcal{H}}_f = \mathcal{T}_f(\widetilde{A}, K, -C, I),$$

with I always as an identity matrix of appropriate dimensions. In addition, use is made of an extended observability matrix that is defined by

$$\Gamma_f^\top = \begin{bmatrix} C^\top & (CA)^\top & \dots & (CA^{f-1})^\top \end{bmatrix}.$$

Matrices $\widetilde{\Gamma}_f$, $\widetilde{\mathcal{T}}_f^{\mathrm{u}}$, and $\widetilde{\mathcal{T}}_f^{\mathrm{d}}$ are defined similar to their counterparts without the tilde but with any A, B_{u}, and B_{d} replaced by respectively $\widetilde{A}$, $\widetilde{B}_{\mathrm{u}}$, and $\widetilde{B}_{\mathrm{d}}$.

C. Obtaining the Data Equations

This section presents the essential equations that are required for the derivation of closed-loop SPC implementations, and are referred to as the *data equations*. These equations are derived to help explain the identification of an output predictor for data-driven predictive control.

Using the innovation form (1), the evolution of outputs can be written as a function of a single initial state as well as input, output, disturbance, and innovation trajectories. By starting from $k = i_p$ (see Fig. 2) with prediction window length f this results in the system description

$$\bar{y}_{i_p,f} = \Gamma_f x_{i_p} + \mathcal{T}_f^{\mathrm{u}} \bar{u}_{i_p,f} + \mathcal{T}_f^{\mathrm{d}} \bar{d}_{i_p,f} + \mathcal{H}_f \bar{e}_{i_p,f}, \quad (3)$$

in which $\bar{y}_{i_p,f}^\top = \begin{bmatrix} y_{i_p}^\top & y_{i_p+1}^\top & \dots & y_{i_p+f-1}^\top \end{bmatrix}$ is a vector of f concatenated subsequent outputs. Consequently, $\bar{u}_{i_p,f}$, $\bar{d}_{i_p,f}$, and $\bar{e}_{i_p,f}$ are defined similarly for inputs, disturbances, and innovations.

By iterative application of (2), it is found that

$$\widetilde{\mathcal{H}}_f \bar{y}_{i_p,f} = \widetilde{\Gamma}_f x_{i_p} + \widetilde{\mathcal{T}}_f^{\mathrm{u}} \bar{u}_{i_p,f} + \widetilde{\mathcal{T}}_f^{\mathrm{d}} \bar{d}_{i_p,f} + \bar{e}_{i_p,f}. \quad (4)$$

For the purpose of data-driven control it is desirable to reduce the effect of terms that are not directly measurable like the initial state, which in (3) and (4) is x_{i_p}. To this end, the state x_{i_p} is expressed in terms of another initial state x_i that lies a past window length p samples back in time (see Fig. 2). By iterative application of (2a) from $k = i$ until $k = i_p = i + p$:

$$x_{i_p} = \widetilde{A}^p x_i + \widetilde{\mathcal{K}}_p^{\mathrm{u}} \bar{u}_{i,p} + \widetilde{\mathcal{K}}_p^{\mathrm{d}} \bar{d}_{i,p} + \widetilde{\mathcal{K}}_p^{\mathrm{y}} \bar{y}_{i,p}, \quad (5)$$

with the reversed extended controllability matrices

$$\widetilde{\mathcal{K}}_p(\mathcal{B}) = [\widetilde{A}^{p-1}\mathcal{B} \ \cdots \ \widetilde{A}\mathcal{B} \ \mathcal{B}],$$
$$\widetilde{\mathcal{K}}_p^{\mathrm{d}} = \widetilde{\mathcal{K}}_p(B_{\mathrm{d}}), \quad \widetilde{\mathcal{K}}_p^{\mathrm{y}} = \widetilde{\mathcal{K}}_p(K), \quad \widetilde{\mathcal{K}}_p^{\mathrm{u}} = \widetilde{\mathcal{K}}_p(B_{\mathrm{u}}).$$

Since all of the eigenvalues of $\widetilde{A}$ are inside the unit circle, a common assumption in subspace identification that is used here is that p is sufficiently large to ensure $\widetilde{A}^p \approx 0$ [26].

By applying (5) to (3) and (4), and by neglecting the contribution of x_i because of the aforementioned assumption, the following data equations are obtained:

$$\begin{aligned} \bar{y}_{i_p,f} = {} & \Gamma_f \widetilde{\mathcal{K}}_p^{\mathrm{u}} \bar{u}_{i,p} + \Gamma_f \widetilde{\mathcal{K}}_p^{\mathrm{d}} \bar{d}_{i,p} + \Gamma_f \widetilde{\mathcal{K}}_p^{\mathrm{y}} \bar{y}_{i,p} \\ & + \mathcal{T}_f^{\mathrm{u}} \bar{u}_{i_p,f} + \mathcal{T}_f^{\mathrm{d}} \bar{d}_{i_p,f} + \mathcal{H}_f \bar{e}_{i_p,f}, \end{aligned} \quad (6)$$

$$\begin{aligned} \widetilde{\mathcal{H}}_f \bar{y}_{i_p,f} = {} & \widetilde{\Gamma}_f \widetilde{\mathcal{K}}_p^{\mathrm{u}} \bar{u}_{i,p} + \widetilde{\Gamma}_f \widetilde{\mathcal{K}}_p^{\mathrm{d}} \bar{d}_{i,p} + \widetilde{\Gamma}_f \widetilde{\mathcal{K}}_p^{\mathrm{y}} \bar{y}_{i,p} \\ & + \widetilde{\mathcal{T}}_f^{\mathrm{u}} \bar{u}_{i_p,f} + \widetilde{\mathcal{T}}_f^{\mathrm{d}} \bar{d}_{i_p,f} + \bar{e}_{i_p,f}. \end{aligned} \quad (7)$$

Essentially, the two above data equations are representations of the same system using different Markov parameters. Since $\widetilde{\mathcal{H}}_f$ is invertible it is clear that [27]

$$\begin{bmatrix} \Gamma_f \widetilde{\mathcal{K}}_p^{\mathrm{z}} & \mathcal{T}_f^{\mathrm{u}} & \mathcal{T}_f^{\mathrm{d}} & \mathcal{H}_f \end{bmatrix} = \widetilde{\mathcal{H}}_f^{-1} \begin{bmatrix} \widetilde{\Gamma}_f \widetilde{\mathcal{K}}_p^{\mathrm{z}} & \widetilde{\mathcal{T}}_f^{\mathrm{u}} & \widetilde{\mathcal{T}}_f^{\mathrm{d}} & I \end{bmatrix}, \quad (8)$$

in which $\widetilde{\mathcal{K}}_p^{\mathrm{z}} = \begin{bmatrix} \widetilde{\mathcal{K}}_p^{\mathrm{y}} & \widetilde{\mathcal{K}}_p^{\mathrm{u}} & \widetilde{\mathcal{K}}_p^{\mathrm{d}} \end{bmatrix}$. This important result indicates that it is possible to switch between representations that are parameterized by the left and right and sides of (8), which will prove useful when forming an output predictor.

D. Forming an Output Predictor

The data equations from the previous section both contain past data from two different data windows that are illustrated in green and blue by Fig. 2. With reference to this figure, the idea of this section is to derive a causal predictor of future outputs $\hat{\bar{y}}_{\hat{i}_p,f}$ by identifying how past outputs in the blue section could best be predicted by input, output and disturbance data from the green window as well as input and disturbance data from the blue window.

In line with this idea, based on (6) an output predictor is proposed of the form

$$\hat{\bar{y}}_{\hat{i}_p,f} = \widehat{\Gamma_f \widetilde{\mathcal{K}}_p^{\mathrm{z}}} \bar{z}_{\hat{i},p} + \widehat{\mathcal{T}}_f^{\mathrm{d}} \bar{d}_{\hat{i}_p,f} + \widehat{\mathcal{T}}_f^{\mathrm{u}} \bar{u}_{\hat{i}_p,f}, \quad (9)$$

in which $\bar{z}_{\hat{i},p}^\top = \begin{bmatrix} \bar{y}_{\hat{i},p}^\top & \bar{u}_{\hat{i},p}^\top & \bar{d}_{\hat{i},p}^\top \end{bmatrix}$, and the $\hat{(\cdot)}$-notation indicates estimated or predicted matrices and vectors. The positions of indices $\hat{i}$ and $\hat{i}_p = \hat{i} + p$ are shown in Fig. 2.

With reference to the same figure, one of the distinguishing features of *closed-loop* SPC is that identification is performed with a prediction window of $f_{\mathrm{ID}} = 1$. This corresponds to only considering the top block-row of one of the data-equations (note that the top block-rows are identical). The reason for using only the top block-row is that this ensures that during closed-loop operation, the inputs and noise that are used for identification remain uncorrelated. Hence, this method prevents identification bias that may negatively influence the performance of the controller [19]. The rest of the output predictor will be constructed from the predictor Markov parameters that are estimated by a least squares problem using the first block-row of the data equations:

$$\begin{bmatrix} \widehat{C\widetilde{\mathcal{K}}_p^{\mathrm{z}}} & \widehat{D_{\mathrm{u}}} & \widehat{D_{\mathrm{d}}} \end{bmatrix} = \arg\min_L \left\| Y_{i_p,1,N} - L \begin{bmatrix} Z_{i,p,N} \\ U_{i_p,1,N} \\ D_{i_p,1,N} \end{bmatrix} \right\|_{\mathrm{F}}^2, \quad (10)$$

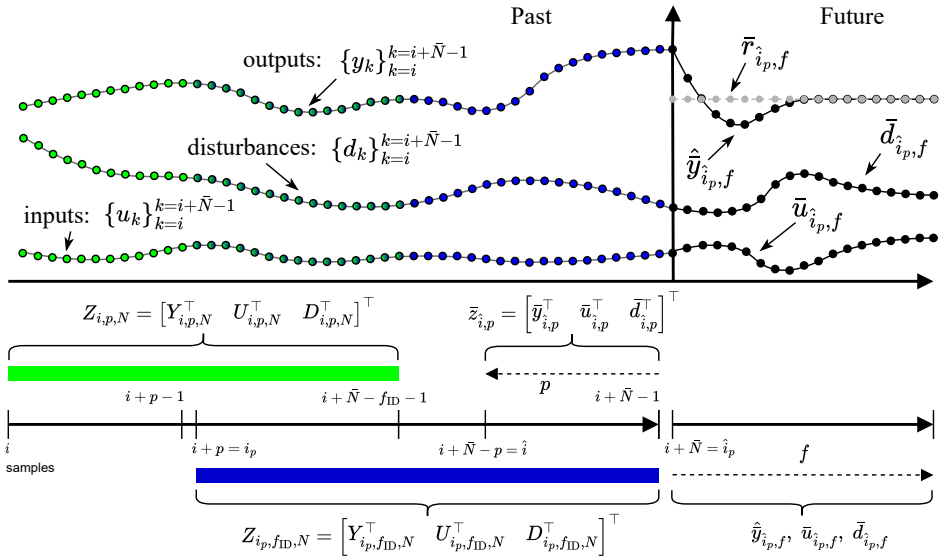

Fig. 2: The relevant past and future data windows in SPC. An output predictor is inferred from the past blue and green data windows. The total number of past data samples used for identification is $\bar{N} = p + f_{\mathrm{ID}} + N - 1$. In regular SPC, $f_{\mathrm{ID}} = f$ whilst in closed-loop SPC identification is performed with $f_{\mathrm{ID}} = 1$ and an output predictor $\hat{\bar{y}}_{\hat{i}_p,f}$ with prediction window length f is constructed (often recursively). An optimal input trajectory can then be computed given a suitable cost function. Closed-loop SPC uses $f_{\mathrm{ID}} = 1$ to avoid closed-loop identification bias due to correlation between inputs and noise, and has as an extra advantage that less data is needed.

in which $Z_{i,p,N} = \begin{bmatrix}\bar{z}_{i,p} & \bar{z}_{i+1,p} & \cdots & \bar{z}_{i+N-1,p}\end{bmatrix}$ is a matrix that is composed of three so-called block-Hankel data matrices that in turn are composed of past outputs, inputs, and disturbances from the green data window in Fig. 2. The block-Hankel data matrices $Y_{i_p,1,N}$, $U_{i_p,1,N}$ and $D_{i_p,1,N}$ are defined similarly to $Z_{i,p,N}$ for respectively past outputs, inputs and disturbances from the blue data window. Moreover, L is an optimization variable, and the subscript F indicates the Frobenius norm. There is a unique solution to the identification problem solved by (10) if the input and disturbance data is sufficiently persistently exciting [28].

Using these estimated predictor Markov parameters it is only possible to directly construct the first block-row of the output predictor given by (9). However, with these parameters and the approximation that $\widetilde{A}^p \approx 0$, it is straightforward to construct all of the matrices on the right hand side of (8). Equation (8) thus demonstrates a method to obtain estimates of the matrices used in (9) from similar matrices that depend on the identified predictor Markov parameters. In practice a recursive method can be employed (see [20]).

E. Finding the Unconstrained Optimal Input

With the output predictor (9) from the previous section, this section derives the optimal input in an unconstrained setting. The cost function that is to be minimized is:

$$\begin{aligned} J =& (\hat{\bar{y}}_{\hat{i}_p,f} - \bar{r}_{\hat{i}_p,f})^\top Q_{\mathrm{a}} (\hat{\bar{y}}_{\hat{i}_p,f} - \bar{r}_{\hat{i}_p,f}) \\ &+ \bar{u}_{\hat{i}_p,f}^\top R_{\mathrm{a}} \bar{u}_{\hat{i}_p,f} + \Delta \bar{u}_{\hat{i}_p,f}^\top R_{\mathrm{a}}^\Delta \Delta \bar{u}_{\hat{i}_p,f}, \end{aligned} \tag{11}$$

in which Q_{a} is a positive semi-definite weighting matrix that penalizes anticipated future output deviations from a reference trajectory $\bar{r}_{\hat{i}_p,f}$, and R_{a} and R_{a}^Δ are input weighting matrices that penalize the absolute input magnitude and the input increments, respectively. For the latter two matrices, at least one has to be positive definite with the other positive (semi-)definite, and without loss of generality it is assumed that all weighting matrices are symmetric. The variable $\Delta \bar{u}_{\hat{i}_p,f}$ represents a vector of incremental future input changes that is given by

$$\Delta \bar{u}_{\hat{i}_p,f} = S_\Delta \bar{u}_{\hat{i}_p,f} - S_{\mathrm{z}} \bar{z}_{\hat{i},p}, \tag{12}$$

$$\text{with } S_\Delta = \begin{bmatrix} I & 0 & \cdots & 0 \\ -I & I & \cdots & 0 \\ \vdots & \ddots & \ddots & \vdots \\ 0 & \cdots & -I & I \end{bmatrix}, \text{ and } S_{\mathrm{z}} = \begin{bmatrix} 0 & I & 0 \\ 0 & 0 & 0 \\ \vdots & \vdots & \vdots \\ 0 & 0 & 0 \end{bmatrix},$$

such that the top block-row of $S_z \bar{z}_{\hat{i},p}$ yields $u_{\hat{i}_p-1}$.

By substituting (9) into (11) the cost function can hence be reformulated as an unconstrained quadratic programming minimization problem:

$$J = \frac{1}{2} \bar{u}_{\hat{i}_p,f}^\top H \bar{u}_{\hat{i}_p,f} + c^\top \bar{u}_{\hat{i}_p,f}, \tag{13a}$$

$$H = (\widehat{\mathcal{T}}_f^{\mathrm{u}})^\top Q_{\mathrm{a}} \widehat{\mathcal{T}}_f^{\mathrm{u}} + R_{\mathrm{a}} + S_\Delta^\top R_{\mathrm{a}}^\Delta S_\Delta, \tag{13b}$$

$$\begin{aligned} c^\top =& \left(\widehat{\Gamma_f \widetilde{\mathcal{K}}_p^{\mathrm{z}}} \bar{z}_{\hat{i},p} + \widehat{\mathcal{T}}_f^{\mathrm{d}} \bar{d}_{\hat{i}_p,f} - \bar{r}_{\hat{i}_p,f}\right) Q_{\mathrm{a}} \widehat{\mathcal{T}}_f^{\mathrm{u}} \\ &- \left(S_{\mathrm{z}} \bar{z}_{\hat{i},p}\right)^\top R_{\mathrm{a}}^\Delta S_\Delta, \end{aligned} \tag{13c}$$

which results in an analytical expression for the optimal input solution trajectory as $\bar{u}_{\hat{i}_p,f}^* = -H^{-1}c$. Since only the first calculated optimal input is implemented in a receding horizon fashion the relevant computation is given using MATLAB notation by

$$u_{\hat{i}_p}^* = -H^{-1}(1:r,:)c. \tag{14}$$

F. Relation to Traditional Closed-Loop SPC

It is now possible to see how the traditional closed-loop SPC controller is retrieved if past and future disturbances are not considered measured quantities. In such a case the identification problem formulated by (10) does not contain disturbance information, so $C\widetilde{\mathcal{K}}_p^{\mathrm{d}}$ and D_{d} are not estimated and the output predictor does not rely on estimates of $\mathcal{T}_f^{\mathrm{d}}$ and $\Gamma_f\widetilde{\mathcal{K}}_p^{\mathrm{d}}$. Without disturbance information, the optimal solution presented by (14) relies on a vector c that is constructed by omitting these terms in (13c) (note that $\Gamma_f\widetilde{\mathcal{K}}_p^{\mathrm{z}}$ then also does not contain $\Gamma_f\widetilde{\mathcal{K}}_p^{\mathrm{d}}$).

III. Data-driven wind turbine simulation

This section demonstrates the performance of the presented closed-loop SPC controller as applied to rotor speed regulation of a wind turbine operating at rated power conditions and that is subject to two different wind cases. The performance of the closed-loop SPC controller is compared for different levels of supplied past and future wind speed information.

A. Simulated Wind Turbine Model

To showcase the potential of the presented method it is important to satisfy the premises and assumptions of the derivation in Section II. Since the closed-loop SPC framework is based on LTI systems, time-marching simulations are performed in MATLAB on an LTI system, obtained by linearizing a nonlinear physical model. Choosing an LTI simulation model enables us to explore the attainable performance levels of the control method and to validate the correctness of the algorithm's implementation.

To this end, the considered system is the NREL 5-MW reference wind turbine model [29], which is linearized at the turbine's rated rotor speed of $\omega_{\mathrm{r}}^* = 12.1$ RPM, a pitch angle of $\beta^* = 17.0^\circ$, a wind speed of $U^* = 20$ m/s, a resultant tip-speed-ratio of 4.0, and a constant rated generator torque of 43.1 kNm. This operating point has been chosen because it constitutes an equilibrium for the nonlinear rotational speed dynamics.

The discrete-time wind turbine model is given in innovation form by

$$\Delta\omega_{\mathrm{r},k+1} = A\Delta\omega_{\mathrm{r},k} + B_{\mathrm{u}}\Delta\beta_{k-\delta} + B_{\mathrm{d}}\Delta U_k + Ke_k, \quad (15a)$$

$$\Delta\omega_{\mathrm{rm},k} = C\Delta\omega_{\mathrm{r},k} + D_{\mathrm{u}}\Delta\beta_{k-\delta} + D_{\mathrm{d}}\Delta U_k + e_k, \quad (15b)$$

in which Δ indicates deviations from the linearization point, $\omega_{\mathrm{r},k}$ is the rotor's actual rotational speed (rad/s), $\omega_{\mathrm{rm},k}$ is the rotor's measured speed (rad/s), β_k is the pitch angle (rad), U_k is the wind speed (m/s), and e_k is ergodic zero-mean white measurement noise with a variance of $1 \cdot 10^{-10}$ rad^2/s^2. To simulate pitch actuator dynamics, the pitch angle is delayed by $\delta = 15$ samples. To capture relevant system dynamics, the step size of the discrete model is $\Delta t = 0.01$ s and the matrices of the system are given by

$$A = 0.9971, \quad B_{\mathrm{u}} = -0.01412, \quad B_{\mathrm{d}} = 0.0002899, \quad K = 0$$
$$C = 1, \qquad D_{\mathrm{u}} = 0, \qquad D_{\mathrm{d}} = 0.$$

Note that the noise of the above model acts purely as additive measurement noise.

B. Simulation and Controller Configurations

The wind turbine model and controllers are simulated within MATLAB. Rotational speed regulation to the rated speed (so as reference for predicted values of $\Delta\omega_{\mathrm{r},k}$ all elements of $\bar{r}_{\hat{i}_p,f}$ are 0 rad/s) is performed subject to a wind speed disturbance signal ΔU_k. Pitch, wind speed and measured rotational speed data that is used by the controllers is provided with respect to the linearization point: $\Delta\beta_k$, ΔU_k, and $\Delta\omega_{\mathrm{rm},k}$.

Two wind cases are simulated. In the first wind case (WC I), the wind speed signal is a Mexican hat profile that occurs in a time window of 5 seconds with a maximum deviation of 7 m/s from the operating point U^*. The second wind case (WC II) consists of a 15 minute long turbulent wind signal with a mean of U^*, a Kaimal turbulence spectrum and an intensity of 15%.

The closed-loop SPC algorithm performance in terms of disturbance attenuation is assessed for different levels of past and future wind speed information. The first controller uses both past and future, previewed wind speed information - akin to accurate LIDAR feedforward - and is referred to as FB+FF. The second controller relies only on feedback and has no knowledge of any wind speeds, past or future (FB). The third controller uses past wind speed data and assumes that all future wind speeds are equal to the last measured wind speed (FB+), which is representative of using accurate anemometer measurements. All controllers use window lenghts $p = 20$, $f = 50$, and $N = 480$ block-Hankel data matrix columns for identification of the predictor Markov parameters. This identification step is performed once after $\bar{N} + \delta$ samples (so after 5.14 s) of persistently exciting ergodic zero mean white noise inputs $\Delta\beta_k$ and disturbances ΔU_k with respectively variances of 0.001 rad^2 and 0.1 m^2/s^2. Since the subsequent, closed-loop data is not guaranteed to be persistently exciting, the identification is performed only once. The chosen weights of the cost function are $Q_{\mathrm{a}} = 1 \cdot 10^5$, $R_{\mathrm{a}} = 0$, and $R_{\mathrm{a}}^{\Delta} = 1$, and the controllers apply the unconstrained optimal control law described by (13) and (14).

C. Simulation Results

The results of the simulation with the three closed-loop SPC controllers for WC I is shown in Fig. 3a. With reference to this figure, it is clear that after a sequence of persistently exciting data for initialization and identification all controllers initially regulate the rotational speed to its rated value. However, the wind speed disturbance induces clear differences in controller performance, with increasing levels of past and future wind speed information leading to more effective wind speed disturbance rejection for rotor speed regulation. The FB+FF controller shows almost perfect disturbance rejection resulting in a tight rotor speed tracking at its rated value. This control performance is attained by starting to pitch earlier than is the case with the FB controller,

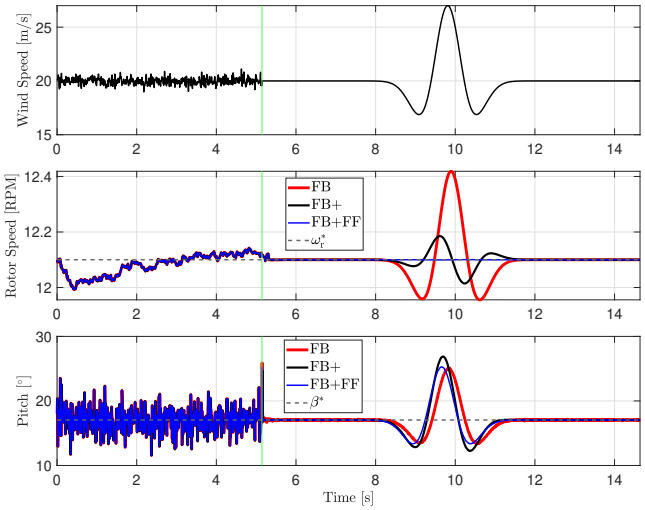

(a) WC I: Mexican hat wind gust disturbance following a section of persistently exciting data to initialize the controller.

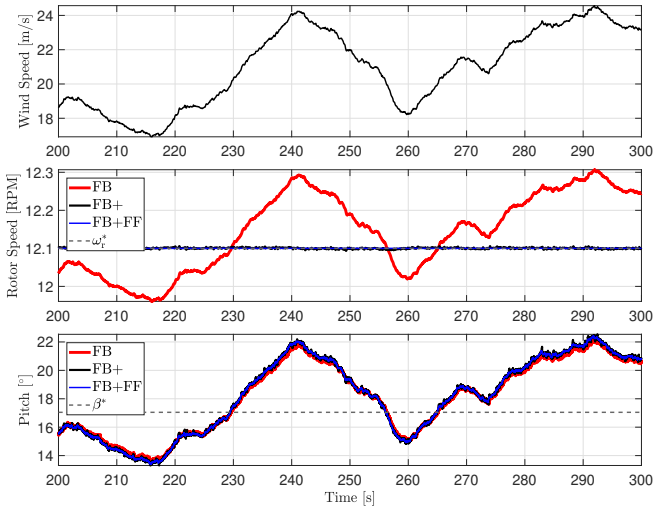

(b) WC II: wind speed profile with turbulence intensity of 15%. Only part of the 15 minute simulation is shown for clarity.

Fig. 3: Above-rated rotational speed regulation capabilities of three closed-loop SPC algorithms. Results for wind case I are shown by (a) and results for wind case II are shown by (b). Wind speed disturbance rejection and speed regulation improves with increasing exploitation of wind speed information (from FB to FB+ and then FB+FF). For clarity only the actual rotational speed is shown since the measurement error is fairly small.

which uses no wind speed previewing. The FB+ controller also reduces the rotational speed fluctuation compared to the FB case by early pitch actuation, but this reduction is less compared to that obtained with the FB+FF controller.

Results demonstrating the performance of the three controllers for WC II are shown in Fig. 3b. As with the previous wind case, it is clear that increasing the degree of past and future wind speed information improves controller performance in terms of rotational speed regulation. The difference between the FB+ and FB+FF controllers is however relatively small when both are compared to the FB case. This is attributable to the fact that the FB controller does not account for the wind speed disturbance, of which the effect is attributed to zero-mean white noise during identification. As such it does not compensate for its effect, and is therefore not able to regulate the rotational speed to its rated value.

To quantify and compare the amount of pitch actuator use we employ the actuator duty cycle (ADC) measure [30]:

$$ADC = \frac{1}{T}\int_0^T \frac{|\dot{\beta}|}{\dot{\beta}_{\max}} \mathrm{d}t, \tag{16}$$

in which T is the length of the considered time window, $\dot{\beta}$ is the pitching rate, and $\dot{\beta}_{\max}$ is the maximum absolute pitching rate, which is taken to be $8^\circ/\mathrm{s}$ here. For WC I the ADC between 7.31 s and 12.31 s of the FB, FB+, and FB+FF controllers is respectively 127.7%, 101.8%, and 85.2%. Although it may appear in Fig. 3a that the FB+ controller uses the most pitch actuation, smaller deviations that are not as well visible for the FB controller mean that it uses the most pitch actuation. Over the 15 minute simulation time for WC II, the FB, FB+, and FB+FF controllers likewise have an ADC of respectively 89.6%, 32.3%, and 21.8%. This demonstrates that increasing wind speed information is benefitial not only for rotor speed regulation, but can also help reduce pitch actuator use.

The underlying cause for the increase in performance with increasing wind speed information is twofold. Firstly, having access to past wind speed information helps obtain a more accurate output predictor since the linear regression problem (10) is better tailored to the actual data equation, which represents the system's dynamics. In effect, for the FB controller, the initial wind speed disturbance that the other controllers use for identification simply adds more noise to the identification problem. This explains why, particularly with a nonzero wind speed disturbance as is shown in Fig. 3b, the FB+ controller is able to outperform the FB controller. Secondly, suboptimal (future) wind speed information also directly leads to a suboptimal control law as per (13) and (14). This is nicely demonstrated by the smaller and leading pitch signal of the FB+FF controller in Fig. 3a when compared to the FB+ controller.

IV. CONCLUSIONS

This work presents a closed-loop SPC algorithm that is able to handle past and future disturbance information. The presented data-driven controller is particularly data-efficient because for identification, with reference to Fig. 2, the window length $f_{\mathrm{ID}} = 1$ (instead of $f_{\mathrm{ID}} = f$), which reduces the total number of past data samples $\bar{N}$. Since this avoids correlation between inputs and noise in closed-loop operation the identification retains consistent estimates with which to ultimately formulate a control law.

The derived controller (FB+FF) is used to regulate the rotational speed of an NREL 5-MW reference wind turbine. Two wind cases are investigated: a wind gust and turbulent wind speed signal and the performance of the presented con-

troller is compared to the closed-loop SPC implementation that employs no wind speed information (FB) or relies on the assumption that future wind speeds are all the same as the last measured wind speed (FB+). The identification of a disturbance model along with the more accurate future wind speed information allows the shown FB+FF controller to clearly outperform both its FB and FB+ counterparts. The FB+FF controller's pitch signal leads the pitch signals of the other controllers to nearly perfectly reject the wind speed disturbance and keep the rotor speed at its rated value by using less pitch actuation, demonstrating the potential of a clear phase advantage that is attributable to wind speed previewing.

Since the derivation of the presented controller assumes that the system to be controlled is LTI this work has considered a linearized wind turbine system. Future work will therefore consider the application of this controller to higher fidelity, nonlinear wind turbine models. Moreover, subsequent work may find it worthwhile to consider applying this controller to multi-variable wind turbine systems and implement constraints within the presented framework.

REFERENCES

[1] P. Veers, K. Dykes, E. Lantz, S. Barth, C. L. Bottasso, O. Carlson, A. Clifton, J. Green, P. Green, H. Holttinen, D. Laird, V. Lehtomäki, J. K. Lundquist, J. Manwell, M. Marquis, C. Meneveau, P. Moriarty, X. Munduate, M. Muskulus, J. Naughton, L. Pao, J. Paquette, J. Peinke, A. Robertson, J. Sanz Rodrigo, A. M. Sempreviva, J. C. Smith, A. Tuohy, and R. Wiser, "Grand challenges in the science of wind energy," *Science*, vol. 366, no. 6464, p. eaau2027, Oct. 2019.

[2] M. S. Khaniki, D. Schlipf, and P. W. Cheng, "A Comparison Between LIDAR-Based Feedforward and DAC for Control of Wind Turbines," in *2018 IEEE Conference on Control Technology and Applications (CCTA)*, Aug. 2018, pp. 1650–1655.

[3] F. Dunne, L. Y. Pao, A. D. Wright, B. Jonkman, and N. Kelley, "Adding feedforward blade pitch control to standard feedback controllers for load mitigation in wind turbines," *Mechatronics*, vol. 21, no. 4, pp. 682–690, June 2011.

[4] M. Sinner, V. Petrović, A. Langidis, L. Neuhaus, M. Hölling, M. Kühn, and L. Y. Pao, "Experimental Testing of a Preview-Enabled Model Predictive Controller for Blade Pitch Control of Wind Turbines," *IEEE Transactions on Control Systems Technology*, vol. 30, no. 2, pp. 583–597, Mar. 2022.

[5] D. Schlipf, P. Fleming, F. Haizmann, A. Scholbrock, M. Hofsäß, A. Wright, and P. W. Cheng, "Field Testing of Feedforward Collective Pitch Control on the CART2 Using a Nacelle-Based Lidar Scanner," *J. Phys.: Conf. Ser.*, vol. 555, no. 1, p. 012090, Dec. 2014.

[6] F. Haizmann, D. Schlipf, S. Raach, A. Scholbrock, A. Wright, C. Slinger, J. Medley, M. Harris, E. Bossanyi, and P. W. Cheng, "Optimization of a feed-forward controller using a CW-lidar system on the CART3," in *2015 American Control Conference (ACC)*, July 2015, pp. 3715–3720.

[7] E. J. N. Menezes, A. M. Araújo, and N. S. Bouchonneau da Silva, "A review on wind turbine control and its associated methods," *Journal of Cleaner Production*, vol. 174, pp. 945–953, Feb. 2018.

[8] A. Scholbrock, P. Fleming, D. Schlipf, A. Wright, K. Johnson, and N. Wang, "Lidar-enhanced wind turbine control: Past, present, and future," in *2016 American Control Conference (ACC)*, July 2016, pp. 1399–1406.

[9] A. J. Russell, M. Collu, A. McDonald, P. R. Thies, A. Mortimer, and A. R. Quayle, "Review of LIDAR-assisted Control for Offshore Wind Turbine Applications," *J. Phys.: Conf. Ser.*, vol. 2362, no. 1, p. 012035, Nov. 2022.

[10] T. Wintermeyer-Kallen, M. Basler, T. Konrad, J. Zierath, and D. Abel, "Challenges of applying model-based predictive wind turbine control in the field," *Forsch Ingenieurwes*, vol. 87, no. 1, pp. 119–128, Mar. 2023.

[11] J. H. Laks, L. Y. Pao, and A. D. Wright, "Control of wind turbines: Past, present, and future," in *2009 American Control Conference*, June 2009, pp. 2096–2103.

[12] S. Formentin, K. van Heusden, and A. Karimi, "A comparison of model-based and data-driven controller tuning," *Int. J. Adapt. Control Signal Process.*, vol. 28, no. 10, pp. 882–897, Oct. 2014.

[13] J. Coulson, J. Lygeros, and F. Dörfler, "Data-Enabled Predictive Control: In the Shallows of the DeePC," in *2019 18th European Control Conference (ECC)*. Naples, Italy: IEEE, June 2019, pp. 307–312.

[14] J. C. Willems, P. Rapisarda, I. Markovsky, and B. L. De Moor, "A note on persistency of excitation," *Systems & Control Letters*, vol. 54, no. 4, pp. 325–329, Apr. 2005.

[15] F. Fiedler and S. Lucia, "On the relationship between data-enabled predictive control and subspace predictive control," in *2021 European Control Conference (ECC)*. Delft, Netherlands: IEEE, June 2021, pp. 222–229.

[16] J. W. van Wingerden, S. P. Mulders, R. Dinkla, T. Oomen, and M. Verhaegen, "Data-enabled predictive control with instrumental variables: The direct equivalence with subspace predictive control," in *2022 IEEE 61st Conference on Decision and Control (CDC)*, Cancun, Mexico, Dec. 2022, pp. 2111–2116.

[17] W. Favoreel, B. De Moor, and M. Gevers, "SPC: Subspace Predictive Control," *IFAC Proceedings Volumes*, vol. 32, no. 2, pp. 4004–4009, July 1999.

[18] L. Ljung and T. McKelvey, "Subspace identification from closed loop data," *Signal Processing*, vol. 52, no. 2, pp. 209–215, July 1996.

[19] R. Dinkla, S. P. Mulders, J. W. van Wingerden, and T. Oomen, "Closed-loop Aspects of Data-Enabled Predictive Control," in *IFAC Proceedings Volumes*, ser. 22nd IFAC World Congress, 2023.

[20] J. Dong, M. Verhaegen, and E. Holweg, "Closed-loop Subspace Predictive Control for Fault Tolerant MPC Design," in *IFAC Proceedings Volumes*, ser. 17th IFAC World Congress, vol. 41, 2008, pp. 3216–3221.

[21] S. T. Navalkar, J. W. van Wingerden, E. van Solingen, T. Oomen, E. Pasterkamp, and G. A. M. van Kuik, "Subspace predictive repetitive control to mitigate periodic loads on large scale wind turbines," *Mechatronics*, vol. 24, no. 8, pp. 916–925, Dec. 2014.

[22] N. Mooren, G. Witvoet, and T. Oomen, "Gaussian process repetitive control: Beyond periodic internal models through kernels," *Automatica*, vol. 140, p. 110273, June 2022.

[23] G. J. van der Veen, "Identification of wind energy systems," Ph.D. dissertation, Delft University of Technology, Delft, Netherlands, 2013.

[24] R. Kadali, B. Huang, and A. Rossiter, "A data driven subspace approach to predictive controller design," *Control Engineering Practice*, vol. 11, no. 3, pp. 261–278, Mar. 2003.

[25] L. Ljung, *System Identification: Theory for the User*, 2nd ed. Prentice Hall, 1999.

[26] A. Chiuso, "The role of vector autoregressive modeling in predictor-based subspace identification," *Automatica*, vol. 43, no. 6, pp. 1034–1048, June 2007.

[27] I. Houtzager, J. W. van Wingerden, and M. Verhaegen, "Recursive Predictor-Based Subspace Identification With Application to the Real-Time Closed-Loop Tracking of Flutter," *IEEE Transactions on Control Systems Technology*, vol. 20, no. 4, pp. 934–949, July 2012.

[28] M. Verhaegen and V. Verdult, *Filtering and System Identification: A Least Squares Approach*. Cambridge ; New York: Cambridge University Press, 2007.

[29] J. Jonkman, S. Butterfield, W. Musial, and G. Scott, "Definition of a 5-MW Reference Wind Turbine for Offshore System Development, Tech. Rep. NREL/TP-500-38060, 947422, Feb. 2009.

[30] C. L. Bottasso, F. Campagnolo, and V. Petrović, "Wind tunnel testing of scaled wind turbine models: Beyond aerodynamics," *Journal of Wind Engineering and Industrial Aerodynamics*, vol. 127, pp. 11–28, Apr. 2014.